



Microfibrous TiO₂ supported photocatalysts prepared by metal-organic chemical vapor infiltration for indoor air and waste water purification

Christos Sarantopoulos^{a,*}, Eric Puzenat^b, Chantal Guillard^b, Jean-Marie Herrmann^b, Alain N. Gleizes^a, Francis Maury^a

^aCIRIMAT, CNRS-INPT-UPS, ENSIACET, 118 route de Narbonne, 31077 Toulouse cedex 4, France

^bInstitut de Recherches sur la Catalyse et l'Environnement de Lyon (IRCELYON, UMR CNRS 5256), Université de Lyon 1, 2 Avenue Albert Einstein 69626 Villeurbanne cedex, France

ARTICLE INFO

Article history:

Received 28 January 2009

Received in revised form 19 May 2009

Accepted 23 May 2009

Available online 6 June 2009

Keywords:

MOCVD

MOCVI

Gas phase infiltration

Titanium dioxide

Photocatalysis

Waste water treatment

Air purification

ABSTRACT

The photocatalytic degradation of gaseous (toluene) and aqueous (imazapyr, malic acid, orange G) pollutants over TiO₂ supported photocatalysts is investigated using a batch reactor. A strong influence of the microstructural characteristics of TiO₂ on the decomposition kinetics of the pollutants is found. Well crystallized, porous TiO₂-anatase films grown under low pressure at 400–500 °C by MOCVD on glass plates and by MOCVI on glass micro-fibers are the best heterogeneous photocatalysts, showing the highest activity. We demonstrate a good control of these characteristics by choosing the deposition parameters. Achieving conformal coverage (i.e. good infiltration) of glass micro-fibers by the TiO₂ thin films has also a strong influence on the photocatalytic activity. A correlation between optimal infiltration, film microstructure and photocatalytic activity is established. Strong similarities between optimal photocatalytic decomposition rate in gas and liquid phase were found with respect to the film microstructure and the photocatalyst mass. The total mineralization of the toluene was prevented because of the deactivation of the photocatalyst surface. However the reactivation of the photocatalyst was achieved by UV irradiation under oxygen stream. This allows a long-term use of the photocatalyst.

© 2009 Elsevier B.V. All rights reserved.

1. Introduction

Nowadays the human activity and the modern way of life are responsible for the aggravation of the environmental pollution. Air and water persisting pollutants (non biodegradable) need to be destroyed by efficient, environmental friendly processes. Heterogeneous photocatalysis is a cost efficient process that can be applied to a large variety of waste products such as pesticides, dyes, amino acids and volatile organic compounds (VOC) [1–3]. It is simple to set up, operate and control. The UV activation of the photocatalyst can lead to the total mineralization of the pollutants to produce CO₂ and H₂O. The efficiency of the process is strongly related to parameters such as light wavelength, radiant flux, reaction temperature, catalyst mass and pollutant concentration as well as with the reactor configuration [4]. Polluted air stream charged with 30 g m⁻³ of VOC and of flow rate up to 1500 m³ h⁻¹ can be treated efficiently by photocatalysis.

Titania (TiO₂) is the most commonly used photocatalyst either in the form of powder nanoparticles or as thin films deposited on a solid support. TiO₂-anatase was proved to be the most efficient solid phase for photocatalytic applications [5–7]. Until now, the major drawback for the industrial applications of the photocatalytic process has been the rather high cost of the particle/fluid separation system to be associated with slurry type photo-reactors. Retrieving the ultra fine photocatalyst particles for recycling increases both cost and treatment time. Immobilizing the photocatalyst on inert supports such as plates [8,9], glass fibers [10], carbon [11], beads [12] or membranes [13] allows continuous flow of pollutants. It offers flexibility in photocatalyst handling and transport and is suitable for small, medium and large scale air or water purification systems, e.g. household, buildings, transport vehicles, space stations.

In a previous paper, we have investigated the chemical vapor infiltration using a metal-organic precursor (MOCVI) of TiO₂ films on glass micro-fiber fabrics [14]. The influence of experimental conditions on the film microstructure was studied and preliminary photocatalytic tests on these deposits were reported. In this work we focus more thoroughly on the relation between the film microstructure and photocatalytic activity (PA) against different pollutants (gas and liquid phase). The glass micro-fibers were

* Corresponding author. Current address: IRCELYON, 2 Avenue Albert Einstein 69626 Villeurbanne cedex, France. Tel.: +33 0 4 72 44 54 03; fax: +33 0 4 72 44 53 99.

E-mail address: christos.sarantopoulos@gmail.com (C. Sarantopoulos).

employed as photocatalyst supports in order to develop efficient photocatalytic media (filters) for air and water treatment systems. They offer mechanical flexibility and higher specific surface area compared to flat substrates, beads or honeycomb type supports. Prior to MOCVI experiments on micro-fibrous substrates, TiO₂ films were prepared on flat glass substrates by low pressure MOCVD and submitted to photocatalytic tests in aqueous solutions. This preliminary step made easier the characterization of the deposits whose growth conditions were very close to MOCVI process. We present the results from both studies using flat glass plates and glass micro-fibers as substrates and we compare the crystal structure, the morphology and the photocatalytic activity of TiO₂ films on aqueous and gaseous pollutants.

2. Experimental

2.1. Film preparation

TiO₂ films were grown in an isothermal, isobaric, horizontal low pressure-CVD reactor using borosilicate glass substrates (flat plates and micro-fiber tissue) and Si(1 0 0) wafers. Titanium tetra-iso-propoxide (TTIP) was used as molecular precursor. The mole fraction of TTIP in the gas phase was varied by controlling the various mass flow rates. Details about film preparation are given elsewhere [14,15]. The borosilicate tissue (30 g m⁻²) used as a photocatalyst support was obtained from C.Y.S. Grp. Composites. It is a high void medium (~90% porosity) with pore diameter of 30–100 μm, generated by randomly weaved fibers of 12 μm average diameter. It exhibits relatively large specific surface area (0.13 m² g⁻¹). Under heat treatment, it remains stable up to 800 °C. Its chemical composition is: SiO₂, 54%; Al₂O₃, 15%; CaO, 17%; B₂O₃, 8%; MgO, 5%; R₂O (R = alkali cation) < 0.8%.

2.2. Film characterization

Film crystallinity was studied by X-ray diffraction (XRD). The mean crystal size was determined by applying the Scherrer's equation to the FWHM of XRD lines (1 0 1), (1 1 2), and (2 2 0) of anatase. The microstructure, the grain size and the thickness were analyzed by scanning electron microscopy (SEM). The arithmetical average of the surface roughness (*R_a*) was measured using an optical interferometer. The specific surface area of films elaborated on micro-fibrous substrates was determined by the BET method.

The film mass was calculated by weighing the substrate before and after the deposition experiment. Then, the total surface of the sample was measured. The specific surface of the film was calculated by taking into account solely the mass of the deposited catalyst.

Optical characteristics were determined from transmittance and reflectance experimental spectra using a UV/vis spectrophotometer equipped with an integration sphere. The UV absorption of the TiO₂ films supported on glass plates was calculated at 365 nm using Eq. (1):

$$A(\%) = 1 - R(\%) - T(\%) \quad (1)$$

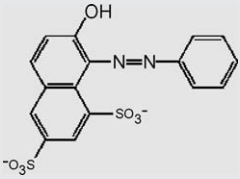
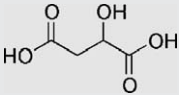
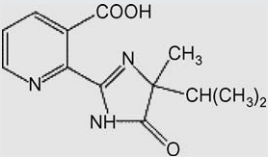
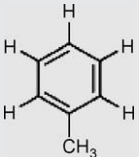
where *A*, *R* and *T* are the absorbance, reflectance and transmittance, respectively. This wavelength corresponds to the principal emission of the UV lamp employed for the photocatalytic tests. The refractive index *n*, the extinction coefficient *k* and the thickness were determined from experimental transmittance spectra using the method of the double envelope [16–18]. Once *n* determined, an average porosity was calculated using Lorentz–Lorentz equation [19]. The surface void percentage of the films was estimated by image analysis of SEM micrographs. It was used as an indication of the open porosity of the films when optical methods could not be applied.

2.3. Photocatalytic tests

2.3.1. Pollutants in aqueous solution

The photocatalytic activity (PA) of the TiO₂ films was initially determined from the degradation of pollutants such as malic acid, imazapyr and orange G in a batch reactor (Table 1). TiO₂-coated borosilicate glass plates (32 mm × 32 mm) were tested with malic acid and imazapyr under 14.5 mW cm⁻² (HPK Philips 125 W lamp, 365 nm). More experimental details are given elsewhere [20,21]. Borosilicate glass plates (20 mm × 20 mm) and fabric samples (30 mm × 20 mm × 0.6 mm) were also tested using an aqueous solution of orange G dye (10⁻⁵ mol L⁻¹). The supported photocatalyst and 25.0 cm³ of the orange G solution were placed into a quartz vessel (28.8 cm³) and irradiated with a flux of 1.05 mW cm⁻² (HPLN Philips 125 W lamp, wavelength 365 nm). The concentration was determined by measuring the absorbance of orange G at 480 nm and by applying Beer–Lambert's law. All solutions were first agitated for 1 h in the dark to reach adsorption equilibrium with the photocatalyst.

Table 1
Experimental conditions of the photocatalytic tests on TiO₂ thin films supported on flat glass substrate and on micro-fibrous borosilicate glass fabric. Some characteristics of pollutants selected as model compounds are reported.

Substance	Orange G ^a	Malic acid ^b	Imazapyr ^b	Toluene ^b
Initial concentration mol L ⁻¹ /(ppm)	10 ⁻⁵ /(4.5)	37.3 × 10 ⁻⁵ /(50)	7.7 × 10 ⁻⁵ /(20)	27.6–110/(30–120)
Molecular Formula	C ₁₆ H ₁₀ N ₂ Na ₂ O ₇ S ₂	C ₄ H ₆ O ₅	C ₁₃ H ₁₅ N ₃ O ₃	C ₇ H ₈
Molecular Structure				
Main use	Industrial textile dye	Oxidation intermediate product	Herbicide	Cigarette, paint, varnish
UV Irradiance (mW cm ⁻²)	1.05	14.50	14.50	14.50
Temperature (°C)	25–35	22–25	22–25	22–25
Substrate	Flat/Glass tissue	Flat glass	Flat glass	Glass tissue
Sample size	20 mm × 20 mm/20 mm × 30 mm × 0.6 mm	32 mm × 32 mm	32 mm × 32 mm	20 mm × 30 mm × 0.6 mm

^a tests performed at CIRIMAT.

^b tests performed at IRCELYON.

2.3.2. Toluene in the gas phase

Photocatalytic tests in the gas phase were carried out using toluene vapor in a batch reactor configuration. The closed circuit was composed of a cylindrical stainless steel reactor (30 mm in diameter, 50 mL), a mixer vessel (250 mL), a gas chromatograph and a peristaltic pump. The TiO₂-coated glass tissue samples (30 mm × 20 mm × 0.6 mm) were placed on a horizontal porous alumina filter (Whatman™) into the reactor. The upper part of the reactor was sealed with a pyrex glass window, transparent to UVA light. The gas phase was continuously recirculated by means of a peristaltic pump under a constant flow rate of 900 mL min⁻¹ (Fig. 1). The photocatalyst was irradiated with 14.5 mW cm⁻² (HPK Philips 125 W lamp, 365 nm). A water-cooling vessel transparent to UVA light was placed between the lamp and the reactor in order to avoid overheating by IR radiation. Before starting the photocatalytic experiment, the gas phase was recirculated in the dark for 1 h in order to reach adsorption equilibrium with the photocatalyst surface. The toluene vapors were generated at a regular rate using a VOC generator. They were mixed with synthetic air (<3 ppm of H₂O, 99.999% pure). The concentration was adjusted at 30, 60 or 120 ppm (or mg per liter of air) by setting the air flow rate at 100, 50 or 25 sccm (standard cubic centimeter per minute) respectively. The gas concentration was analyzed by gas chromatography operating with a flame ionization detector (FID). A capillary CPSil5CB Alltech C-5000 column (Length 25 m; diameter 0.32 mm; stationary phase: dimethylpolysiloxane, 1.2 μm) was used for the toluene analysis. The furnace, the injector and the FID detector temperatures were held at 60, 150 and 200 °C, respectively.

2.3.3. PA determination

The photocatalytic degradation generally follows a Langmuir–Hinshelwood mechanism with the rate r being proportional to the relative coverage θ [4]. In this study we use the initial decomposition rate r_0 to assess the photo-reactivity of the catalyst. r_0 was determined from the slope of the curve of concentration against time in the first minutes of reaction, before any intermediate production modifies the kinetics: typically the first 30 min for the decomposition of malic acid, imazapyr and orange G, and the first 15 min for that of toluene.

3. Results

MOCVD and MOCVI of TiO₂ were performed at 1 and 20 Torr with a total gas flow rate of 600 sccm. The same reactor was used for both deposition processes. The different acronym for each process aims identifying the characteristics of the substrate: flat plates and 3D-porous one, respectively. Changing the growth temperature (300–600 °C) and the precursor mole fraction ($\chi_{\text{TTIP}} = 76, 260$ and 1035×10^{-6}) led to films with different and controllable microstructures.

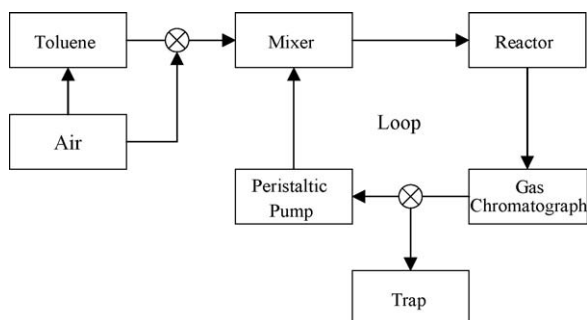


Fig. 1. Scheme of the set up used for gas phase photocatalytic tests.

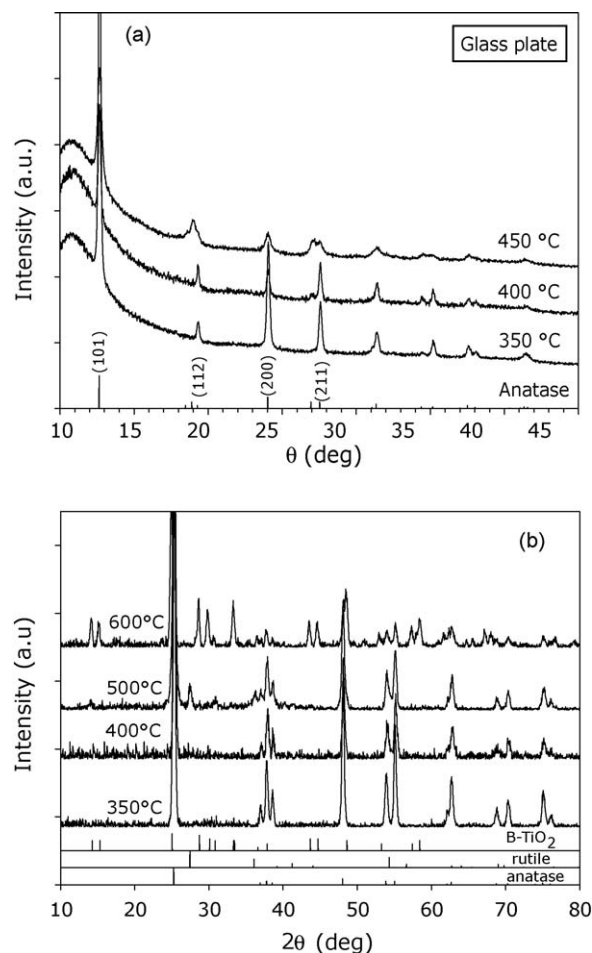


Fig. 2. XRD patterns of TiO₂ layers grown at various temperatures (350–600 °C) on borosilicate glass: (a) flat substrates and (b) fibers (total pressure 20 Torr; TTIP mole fraction 76×10^{-6}).

3.1. Microstructural features of TiO₂ films

3.1.1. Crystalline structure

TTIP mole fraction and growth temperature have a net effect on the allotropic composition of the films. TiO₂ films can grow by TTIP pyrolytic decomposition starting from 220 °C [22]. Operating at high TTIP mole fractions ($260\text{--}1035 \times 10^{-6}$) and low temperatures (300–350 °C) yield pure anatase (Fig. 2a). However, these films are dense. They contain an amorphous phase ($T < 350$ °C). Thus they are not suitable for photocatalytic applications. The film crystallinity improves when increasing the temperature. At 450 °C the films grown on borosilicate glass plates consist of poorly crystallized anatase due to thermal softening of the glass surface (Fig. 2a). Films grown at higher temperatures (500 °C) on the micro-fibrous substrates (more thermally resistant than the glass plates) were mixtures of anatase and rutile (Fig. 2b). From X-ray diffraction lines intensity (peak area) measurements [23] it was deduced that the film grown at 500 °C consisted of 91% of anatase and 9% of rutile. The reflections (1 1 0) of rutile and (1 0 1) of anatase phase were used. The TiO₂ films deposited at 600 °C were light blue which reveals a contamination or a structural change. XRD patterns showed the presence of the bronze-type TiO₂-B phase [24] mixed with anatase. The formation of TiO₂-B most likely results from the diffusion of alkaline ions (e.g. Na⁺) from the glass substrate into the growing oxide. To avoid this harmful diffusion, the growth temperature was kept below 600 °C in the CVD processes. To our knowledge, this is the first report of TiO₂-B phase grown by CVD.

Anatase grown on Si(1 0 0) substrates between 300 and 600 °C exhibits mean crystal sizes increasing from 17 to 51 nm by increasing the temperature. Typically, at 400 °C, the average anatase crystal size is 25 nm. The rutile component of the bi-phased films grown at 500 °C has a comparable grain size of 26 nm. The variation of the TTIP mole fraction has no significant effect on the average crystal size.

3.1.2. Morphology

A way to get porous films, hence to increase the number of photocatalytic active sites, is to favor the columnar growth mode. Three size parameters are introduced in order to assess morphology changes with experimental conditions. Surface grain size (SGS) designates the mean grain size measured on SEM images of the surface, which correspond generally to aggregates of small crystals. In the case of films with columnar morphology, the average of the widths at the bottom and the top of the columns is described by the column mean width (CMW). The third size parameter is the film thickness. CMW and film thickness were measured on SEM cross-sectional micrographs.

The films grown at 300 °C on flat and fibrous substrates had a uniform and compact arrangement of large grains (SGS averaging 225 nm). SEM analysis showed neither film cracking nor evidence of poor adherence. Under this condition, the specific surface area of the films is $1 \text{ m}^2 \text{ g}^{-1}$, as determined by BET. Increasing the temperature led to porous films of columnar morphology. The change of film microstructure was mostly studied for films prepared at 400 °C. As long as the thickness is lower than 400 nm, the films grown on flat substrates show a compact morphology, as evidenced by FEG-SEM images (Fig. 3a). Columnar grains start to grow only beyond this thickness. Their height rises linearly with the deposition time (Fig. 3b). The film growth rate varies from 2.3 to 58 nm min^{-1} , depending on the precursor mole fraction used (76 to 1035×10^{-6} , respectively). The average film roughness (R_a) increases from 4 to 90 nm for film thickness going from 200 nm to 2500 nm, respectively.

The TiO_2 film morphology is reproducible on glass micro-fiber substrates. At 400 °C it covers uniformly the fibers and shows a columnar morphology (Fig. 3c). The porosity of the films elaborated by MOCVD is rather high and depends strongly on the thickness. For film thickness equal to or lower than 300 nm, the porosity is about 18–19% (Fig. 4). Above 300 nm, it increases almost linearly with the thickness and stabilizes to almost 38–40% for films thicker than 1150 nm. The CMW remains small (150–200 nm) even for films of high thickness (2000 nm). Since they grow perpendicular to the highly curved surface of the micro-fibers, the columns do not grow parallel to each other: their inter-distance slightly increases from the bottom to the top as they grow. Therefore, the porosity is expected to be higher compared to films grown on flat glass substrates. To assess the increase in porosity, the surface void percentage was tentatively estimated by image analyzing of SEM micrographs. A flat film with a total porosity of 38% (measured from transmittance spectra) shows a surface void percentage of 27%. The discrepancy between these values comes essentially from the surface void calculation. In the image analysis, the pores are idealistically treated as cylinders perpendicular to the surface with a constant section on their whole length. This means only the open porosity is estimated. The optical methods instead assess the total porosity of the film, including small and closed cavities undetected from surface observation and image analysis. The optically determined porosity leads likely to an overestimation of the porosity exposed to the reactive phase during the photocatalytic tests.

Comparing two films of similar thickness ($\sim 1200 \text{ nm}$), grown on flat and fibrous substrates, showed that the surface void percentage rose from 27 to 50%, respectively. This gives evidence

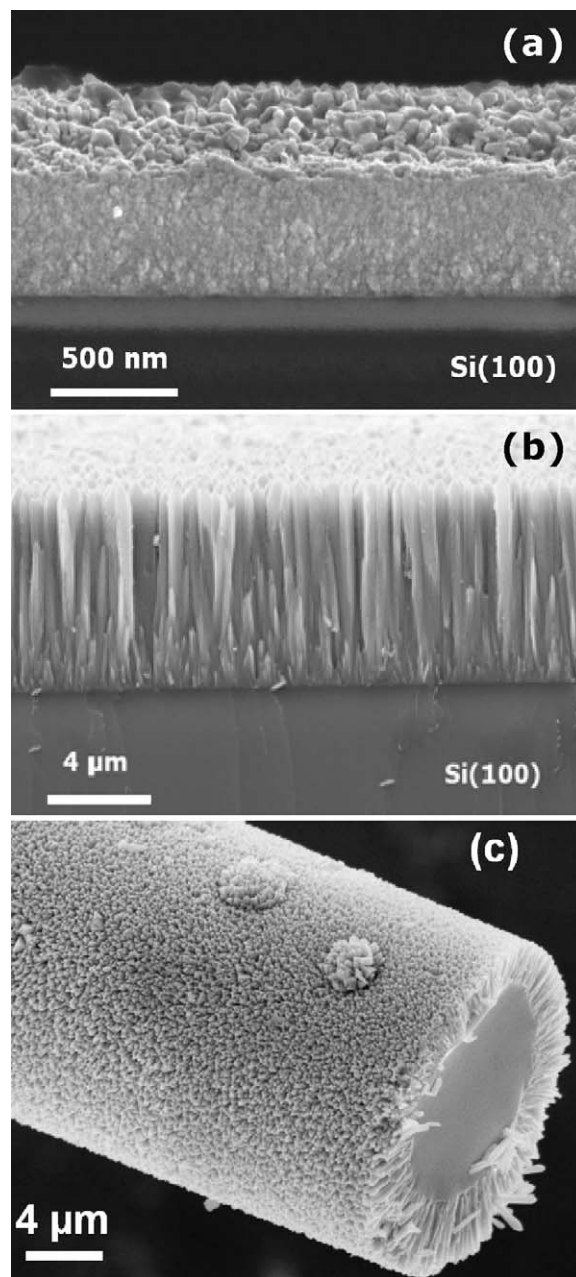


Fig. 3. SEM micrographs of TiO_2 films deposited at 400 °C: (a) thin film (500 nm) on Si(100) before columnar growth be developed; (b) thick film ($\sim 8 \mu\text{m}$) on Si(100); (c) thick film on glass fibers (total pressure 20 Torr; TTIP mole fraction 76×10^{-6}).

for an increase of the total porosity. The porous TiO_2 film (50%) grown on the micro-fibrous substrate also shows a higher specific surface area ($17 \text{ m}^2 \text{ g}^{-1}$), as measured by BET. The CMW increases when the temperature is increased at 500–600 °C. Films thicker than 2000 nm show a dendritic structure. The formation of dendrites increases the surface area but renders the deposits fragile. The TiO_2 -B-rich deposits grown at 600 °C show a columnar morphology with sharp tops.

3.2. Photocatalytic tests in aqueous solution

3.2.1. Effect of the growth temperature

3.2.1.1. Flat substrates. Fig. 5 presents the variation of r_0 for orange G, normalized by the mass of TiO_2 coating (r'_0), for films grown at various temperatures on flat glass plates. The films prepared at

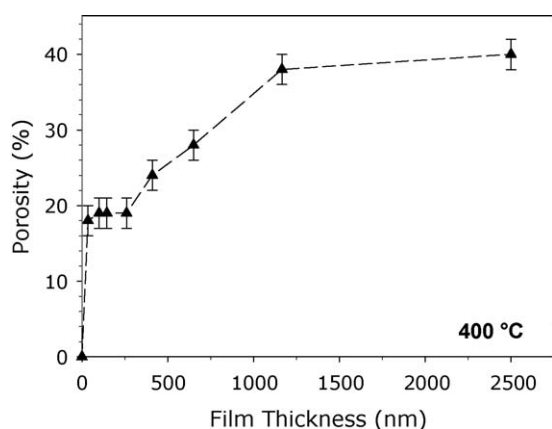


Fig. 4. Variation of total porosity (from optical absorption) as a function of the TiO_2 film thickness. Films were grown at 400°C and 20 Torr using TTIP mole fractions in the range $76\text{--}260 \times 10^{-6}$.

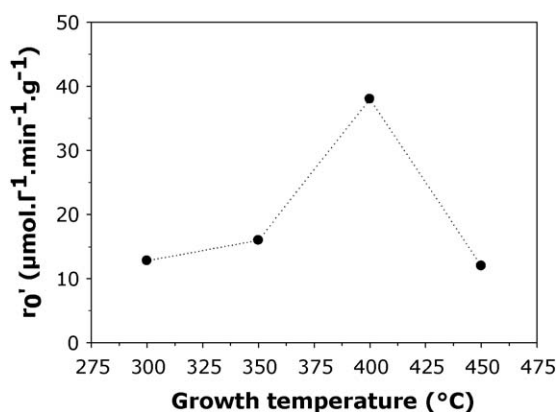


Fig. 5. Variation of the initial decomposition rate of orange G normalized to the mass of TiO_2 (r_0') with the growth temperature. TiO_2 were deposited on flat glass substrates of same dimensions and have comparable thickness.

400°C show the highest PA. This is mainly attributed to the well crystallized and highly porous (38% for 1150 nm thick films) columnar morphology. Conversely, the films grown at lower temperatures are more compact and less well crystallized (broad XRD lines, Fig. 2a), hence they show a lower PA. The films deposited at 450°C are also less photo-reactive because of the poor crystallinity resulting from the onset of thermal softening of the glass (Fig. 2a).

3.2.1.2. Fibrous substrates. Using micro-fiber tissue substrates allowed film deposition at higher temperatures up to 600°C because the glass is less thermal sensitive. Fig. 6 shows the variation of r_0 , normalized by the mass of catalyst (r_0' , left Y-axis), with the growth temperature. The samples prepared between 400 and 500°C present the highest PA. Several factors may contribute to the PA optimization at 500°C : (i) the good crystallinity of the photocatalyst which favors the mobility of the charges; (ii) the low carbon contamination coming from the TTIP precursor; (iii) the high porosity due to the columnar morphology. The presence of small amounts of rutile (less than 10%) in the films prepared at 500°C seems not to significantly influence the PA. This result is in agreement with the work of S.-C Jung et al. [12]. The films prepared at 600°C consist mainly of $\text{TiO}_2\text{-B}$ and of a small fraction of anatase. They show low PA. The band gap energy of $\text{TiO}_2\text{-B}$ is 3.3 eV, corresponding to a wavelength of 376 nm [25]. We conclude that $\text{TiO}_2\text{-B}$ is a less or not efficient photocatalyst compared to anatase.

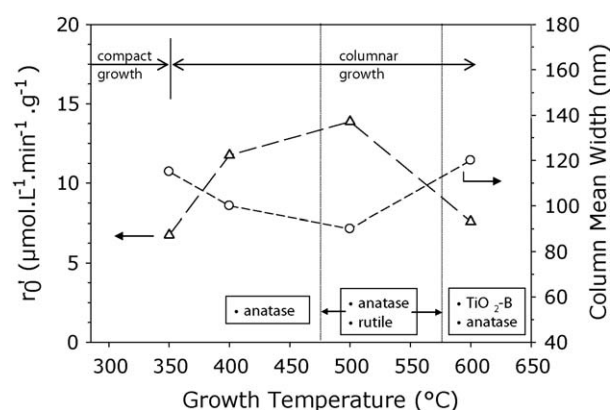


Fig. 6. Variation of the initial decomposition rate of orange G normalized to the mass of TiO_2 (Δ) and of the CMW (\circ) with the growth temperature. TiO_2 were grown on glass fiber fabric of same dimensions and have comparable thickness. Depending on the temperature, the main features of the structure are reported.

3.2.2. Effect of film thickness

3.2.2.1. Flat substrates. Fig. 7a shows the variation of r_0 for malic acid and imazapyr (aqueous solutions) as a function of film thickness. The tested samples were prepared at 400°C , 20 Torr, with a low TTIP mole fraction of 76×10^{-6} , except for the 2500 nm thick sample, for which the mole fraction was set to 260×10^{-6} . r_0 increases with film thickness up to about 750 nm for malic acid and 1150 nm for imazapyr. Beyond these values, r_0 no longer depends on thickness. Testing the same samples with the orange G dye led also to a critical thickness around 1250 nm (Fig. 7b). Observation of a critical thickness was previously reported for

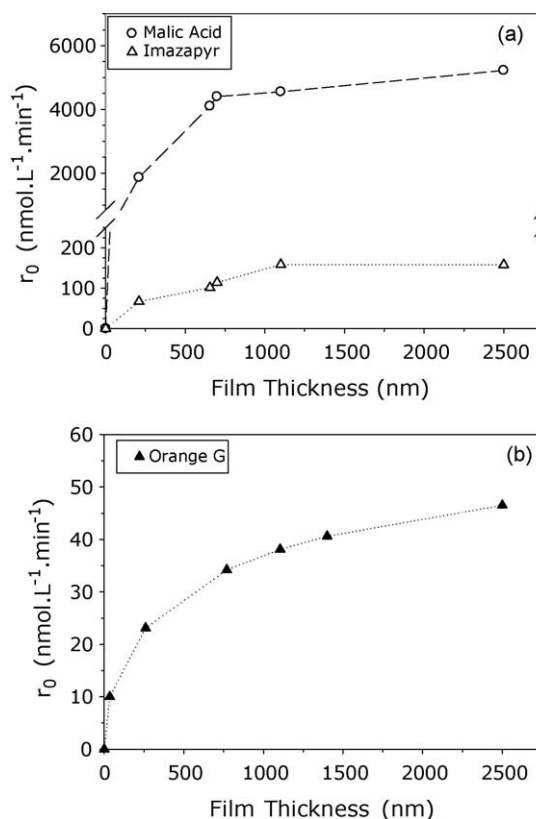


Fig. 7. Variation of r_0 for different pollutants in aqueous solutions with the film thickness: (a) malic acid and imazapyr; (b) orange G. TiO_2 films were deposited at 400°C , 20 Torr using TTIP mole fractions of $76\text{--}260 \times 10^{-6}$ on flat glass substrates ($32\text{ mm} \times 32\text{ mm}$).

plasma and sol gel TiO₂ films [20] in good agreement with our own results for MOCVD layers [9,14].

3.2.2.2. Fibrous substrates. The effect of thickness on the PA of films grown on micro-fibrous substrates was initially studied using the orange G decomposition. The films were prepared at various temperatures in the range 350–500 °C under 20 Torr, with low TTIP mole fractions (76×10^{-6} and 260×10^{-6}). In all cases, r_0 increases almost linearly with film thickness and reaches a plateau above a certain critical thickness (Fig. 6, [14]). This critical thickness varies with the deposition temperature. For films prepared at 350 °C, r_0 is optimized at about 240 nm of thickness. At 400 and 500 °C the plateau is reached at 580 and 660 nm, respectively.

3.2.3. Effect of the microstructure

Two films of same thickness can present different PA depending on their microstructural characteristics. To explain this variation, parameters such as light absorption, film porosity, and average crystal and grain sizes were investigated.

Light absorption and porosity are strongly related to the film thickness. Fig. 8 shows that light absorption increases rapidly at low film thickness and finally stabilizes at 90–95% above 1150 nm. This is related to the depth penetration of the light. This result suggests that for thickness lower than 1150 nm the PA is not limited by the UV light absorption. In other words, the oxide material at depths greater than 1150 nm does not participate to the photocatalytic reaction since beyond this thickness TiO₂ crystallites are not efficiently irradiated by UV light. Depending on film morphology, grain size and porosity, the critical layer thickness of light absorption can vary [26]. Fig. 4 shows that there is no further increase in the film porosity when the layer thickness exceeds 1150 nm. The stabilization of porosity can be a limiting parameter of the photocatalytic reaction because of the ensuing stabilization of the number of the catalytic sites.

In previous works, a size of 7 nm [27] or 50 nm [28] of TiO₂ crystal was proposed for an optimized PA. In this work, the average crystal size of anatase varies from 22 to 40 nm when the growth temperature is raised from 300 to 600 °C, respectively. The optimum PA is obtained for films consisting of crystals of average size between 25 and 36 nm. We suggest that in this range of crystal size the rate of charges recombination between the surface and volume of the crystal is minimized. The increase of the film thickness leads to the formation of larger grains. Fig. 6 presents the variation of the CMW (right Y-axis) with the growth temperature. The CMW decreases when the temperature is increased from 350 to 500 °C, and it increases again beyond 500 °C. The SGS varies in the same way. Taylor et al. reported a similar grain size variation

versus deposition temperature [29]. CMW minimization at 500 °C can account for PA optimization due to the increase of porosity and the decrease of charge recombination inside the grains (90 nm CMW and 54 nm SGS) constituted of small crystals (36 nm).

3.2.4. Effect of the film uniformity (infiltration)

The choice of the experimental conditions for preparing a photocatalyst supported on three-dimensional porous substrate (filter) is a key point [14]. We have shown that the most photocatalytically efficient microstructure is obtained between 400 and 500 °C (Fig. 6).

It is interesting to comparatively study the initial decomposition rate of orange G on two TiO₂-covered fiber tissue samples (20 mm × 30 mm × 0.6 mm) prepared at 300 and 400 °C with the same pressure of 1 Torr and TTIP molar fraction of 5×10^{-3} . The film grown at 300 °C covers uniformly the fibers (good conformal coverage), as result of efficient infiltration. At 400 °C, the reactive gas phase is consumed more readily near the external surface of the 3D-porous substrate, leading to preferential deposition on one side of the glass fabric, and subsequently to a poor infiltration. Comparing the initial decomposition rates normalized by the mass of catalyst shows that the best-covered sample, obtained at 300 °C, is almost six times more active ($r'_0 = 56 \text{ mmol l}^{-1} \text{ min}^{-1} \text{ g}^{-1}$) than the sample prepared at 400 °C ($r'_0 = 9.8 \text{ mmol l}^{-1} \text{ min}^{-1} \text{ g}^{-1}$).

3.3. Photocatalytic tests in air stream

Photocatalytic runs were performed for various initial toluene concentrations in air stream (30, 60 and 120 ppm). Only micro-fibrous supported TiO₂ films were used. Under UV irradiation, toluene decomposes rapidly: the concentration decreases linearly with time during the first 15 min. Then, the decomposition rate slows down and becomes zero. This is likely due to the progressive production of oxidation intermediates and ensuing catalyst deactivation [30,31].

3.3.1. Effect of the initial concentration of toluene

Fig. 9 shows the photocatalytic oxidation of toluene appears to be first order for low pollutant concentrations. This is in agreement with S.B. Kim et al. [32] whereas Luo et al. claimed that between 0.16 and 0.55 ppm of toluene the oxidation rate was between zero and first order [33]. The rate constants of decomposition reaction (k) and of adsorption (K) calculated in the Langmuir–Hinshelwood formalism are $k = 0.0137 \text{ } \mu\text{mol L}^{-1} \text{ min}^{-1}$ and $K = 0.2668 \text{ L mol}^{-1}$, respectively. They differ from values found in the literature most

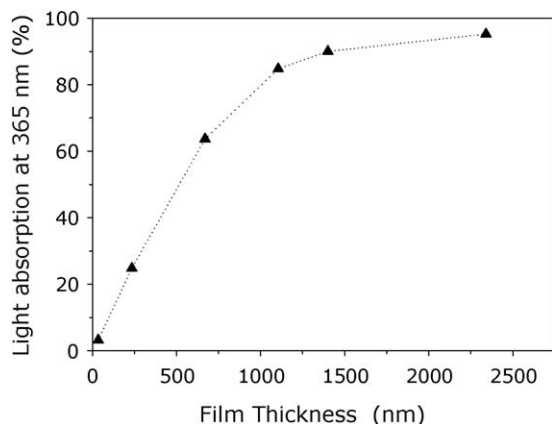


Fig. 8. UV light absorption at 365 nm of TiO₂ layers versus the thickness. Films were elaborated on flat glass substrates at 400 °C, 20 Torr and $76\text{--}260 \times 10^{-6}$ of TTIP.

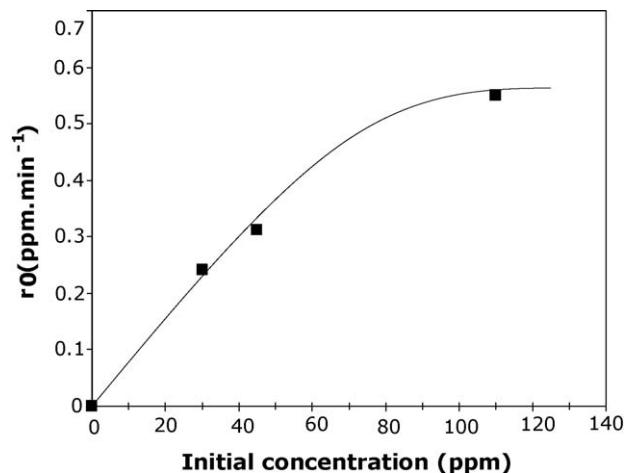


Fig. 9. Effect of the initial concentration of toluene in air stream (ppm) on the initial decomposition rate r_0 .

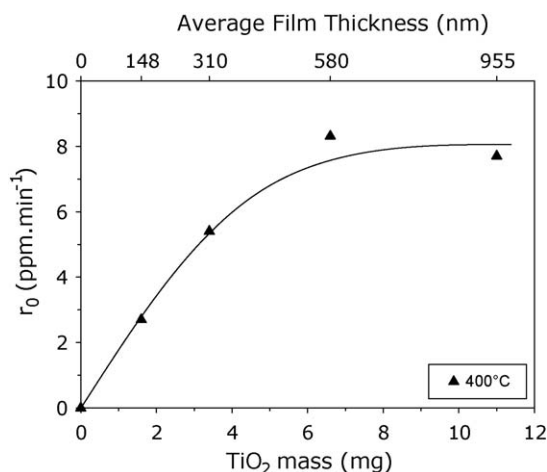


Fig. 10. Variation of r_0 of toluene with the average film thickness (mass of photocatalyst). TiO_2 films were grown at 400°C , 20 Torr using $76\text{--}260 \times 10^{-6}$ of TTIP mole fraction.

probably because of different experimental conditions: light intensity, employment of powder catalyst in fixed bed instead of supported photocatalytic thin film or addition of water vapor in the gas phase [32,33].

3.3.2. Effect of film thickness

The effect of film thickness on the photocatalytic decomposition of toluene vapors was studied using samples prepared at 400°C , 20 Torr, with 76×10^{-6} of TTIP, except for the 995 nm thick one that was grown using 260×10^{-6} . Fig. 10 presents the variation of r_0 with the mass of photocatalyst (lower X-axis) and with the thickness (upper X-axis). r_0 increases quasi linearly with the thickness and reaches a plateau at 580 nm. The stabilization of r_0 is considered to be due to the increase of the grain size or to the porosity stabilization with increasing film thickness.

3.3.3. Effect of the number of catalytic sites

The influence of the photocatalyst distribution on fibrous glass tissues ($20\text{ mm} \times 30\text{ mm} \times 0.6\text{ mm}$) was also studied in gas phase photocatalytic reactions. Two samples are compared. The first sample (T3-1.6) consists of three stacked pieces of fabric and it is infiltrated with 1.6 mg of TiO_2 . The second sample (T1-1.8) consists of only one piece, infiltrated with 1.8 mg of TiO_2 . The average coating thickness is 60 nm for T3-1.6 and 180 nm for T1-1.8, as deduced from the mass of infiltrated TiO_2 and assuming the exposed surface is uniformly coated with TiO_2 . r_0 is identical for the two samples, as shown in Fig. 11. However, after 1 h of UV irradiation, the percentage of decomposed toluene is 65% for T3-1.6 and 55% for T1-1.8. The three-piece sample T3-1.6 is more efficient in terms of pollutant conversion. Since both films are less than 300 nm thick, they show likely the same grain size and porosity. Therefore T3-1.6 is expected to have a higher surface area than the one-piece sample T1-1.8. The higher number of adsorption sites was confirmed by performing isothermal adsorption of toluene vapor on the two samples without UV-A irradiation: T3-1.6 adsorbed more toluene than T1-1.8 (not shown; supplementary material).

3.3.4. Photocatalyst deactivation

One of the biggest challenges in waste treatment is the total mineralization of the organic pollutants. Photocatalysis can achieve this goal. However pollutants such as toluene present in air stream in high concentrations (0–100 ppm) are hard to mineralize into CO_2 and H_2O . Intermediate products of slow

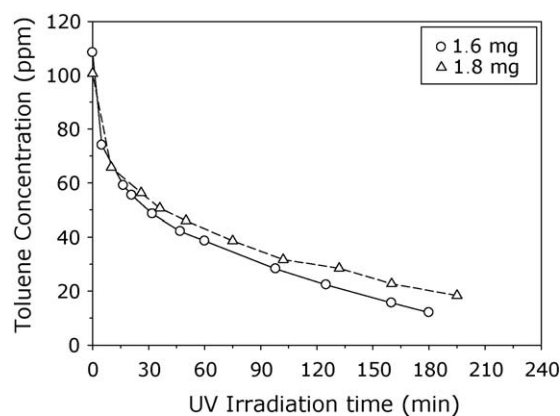


Fig. 11. Kinetic curves of the photocatalytic decomposition of toluene in air stream for two samples of comparable TiO_2 mass but deposited on different number of tissue layers: (○) T3-1.6 (3 layers, 1.6 mg); (△) T1-1.8 (1 layer, 1.8 mg). TiO_2 films were grown at 400°C , 20 Torr using 76×10^{-6} of TTIP mole fraction.

intrinsic decomposition rate are adsorbed on the free catalytic sites, thus deactivating the photocatalyst. Several authors have correlated the photocatalyst deactivation during toluene photocatalytic degradation with the simultaneous yellow bronze-like coloration that appears [30,34]. Adding metallic particles on the photocatalyst surface [35,36], or using reactive gas as water vapor [31,37], can delay surface deactivation. Working with *in situ* FT-IR analysis Mendez-Roman et al. [31] have identified benzoic acid as the intermediate compound responsible for the photocatalyst deactivation.

In the present work, the CO_2 production rate was measured by gas chromatography as an indication of toluene degradation to phenol. Direct mineralization is less probable due to the high number of intermediate compounds. Two samples of supported TiO_2 on glass fiber fabric were used. The sample T3-3.4 consists of 3.4 mg of TiO_2 deposited on three stacked fabric of dimensions $20\text{ mm} \times 30\text{ mm} \times 0.6\text{ mm}$ each, whereas the sample T1-6.6 consists of 6.6 mg of TiO_2 deposited on a single tissue of same dimensions. Average TiO_2 film thickness is 310 nm for T3-3.4 and 580 nm for T1-6.6 as deduced from the mass of infiltrated catalyst. Therefore the deposit is more compact in T3-3.4 and more columnar in T1-6.6: the porosity is 50% higher for T1-6.6 but the photocatalyst surface area is 3 times higher for T3-3.4. Fig. 12 shows that r_0 is higher for T1-6.6 than for T3-3.4. After 150 min of irradiation up to 84% of the toluene is decomposed on T1-6.6 sample while with T3-3.4 the degradation is complete. At this stage, the surface of T1-6.6 is inactive. We conclude that the photocatalyst, even of compact

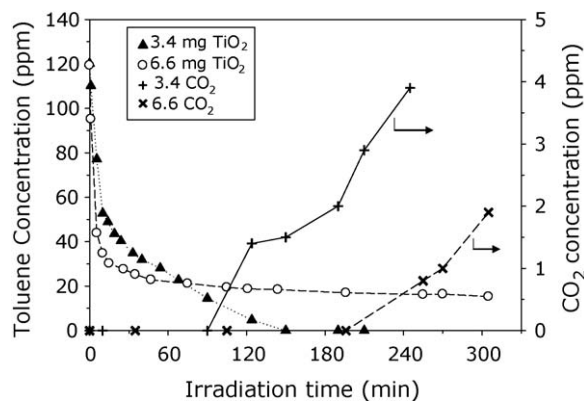


Fig. 12. Kinetic curves of photocatalytic decomposition of toluene in air stream over TiO_2 films supported on glass fiber fabric. Effect of the TiO_2 mass distribution on the CO_2 production and inactivation of the photocatalyst.

Table 2

Comparison of the photocatalytic efficiency (orange G decomposition) of two samples grown under the same conditions on a flat glass substrate and fiber fabric (400 °C; 20 Torr; TTIP mole fraction 76×10^{-6}).

Sample	Mean crystal size (nm)	Critical thickness (nm)	Film porosity (%)	r_0 (nmol L ⁻¹ min ⁻¹) ^a	TiO ₂ mass (mg)	r'_0 (mmol L ⁻¹ min ⁻¹ g ⁻¹) ^b
Flat glass	25	1250	27	40	19	2.1
Fiber fabric	25	600	50	80	7	11.0

^a initial decomposition rate at critical thickness.

^b initial decomposition rate normalized by the mass of TiO₂ at critical thickness.

microstructure, is more efficient when it is dispersed on three pieces of fabric (T3-3.4) than on a single piece (T1-6.6). This is consistent with the results presented above for orange G. For both samples, CO₂ is detected when approximately 88% of the initial toluene concentration has been decomposed. CO₂ is produced faster for T3-3.4 and in larger quantities. This suggests that samples with large photocatalyst distribution, like T3-3.4, are more appropriate for toluene mineralization. The non respect of stoichiometry concerning the decomposition of toluene to CO₂ and phenol is explained by the existence of parallel, still unknown, photocatalytic reaction pathways. The photocatalyst was efficiently reactivated by UVA irradiation (14.5 mW cm⁻²) under oxygen stream for 24 h.

4. Discussion

The development of powerful catalysts requires the consideration and optimization of the microstructural features of the materials. In photocatalysis, an additional parameter must also be considered, the light. In this work we try to understand how we can improve the microstructure of TiO₂ layers and light absorption in order to optimize the PA of the supported photocatalyst. We suggest that a maximal number of photocatalytic active sites on surface should be obtained, i.e. surface sites simultaneously exposed to the pollutant and to UV light. This depends on crystal size and film thickness as well as open porosity provided that the absorption of light is not a limiting step [26].

To demonstrate this, we compare the PA of two samples of supported TiO₂ photocatalyst elaborated under the same conditions on flat and fibrous substrates (Table 2). We also consider that for all samples: (i) the kinetics of decomposition of orange G is the same, and (ii) crystal sizes are identical due to similar deposition conditions (χ_{TTIP} of 76×10^{-6} and growth temperature of 400 °C). The comparison between Fig. 7b of this paper and the Fig. 6 reported in a previous article [14], shows that the critical thickness (which is expected to be related to the depth penetration of light) corresponding to the optimal PA of films grown at 400 °C on flat and fibrous substrates depends on the geometry of the substrate: it is two times smaller for the fibers (600 nm) compared to flat substrate (1250 nm). This difference can be explained by shading effects (absorption of UV light by coated fibers) and scattering phenomena which are expected for the 3D-porous samples.

The initial decomposition rate normalized by the mass of TiO₂ film (r'_0) at the critical thickness characterizes the optimal efficiency of the photocatalyst. From r_0 values found for the plate (Fig. 7b) and the fibers (Fig. 6 of [14]), and the mass of TiO₂ of these samples, the optimal PA at critical thickness is $r'_0 = 2.1$ and $11 \mu\text{mol L}^{-1} \text{min}^{-1} \text{g}^{-1}$, respectively (Table 2). Thus the efficiency of the fiber supported photocatalyst is five times higher than for the plate.

We have also shown that film porosity is almost doubled when using fibrous substrates (from 27% for a flat surface to 50% for the fibers, as determined from image analysis of ~ 1200 nm thick films). By increasing the porosity we expected that a greater part of the film would participate to the photocatalytic reaction, thus

raising the optimal PA by the same factor. Here the higher PA efficiency by a factor five of the fiber cannot be explained only by the increase of the open porosity which increases only by a factor two. Clearly this is the beneficial effect of an increase of the density of photocatalytic active sites, which in turn is related to the specific surface area. A significant increase of the specific surface area is an important requirement to improve the photocatalytic activity. We have seen for instance that a 3D-sample infiltrated at 300 °C is almost six times more active ($r'_0 = 56 \text{ mmol L}^{-1} \text{min}^{-1} \text{g}^{-1}$) than a sample prepared at 400 °C ($r'_0 = 9.8 \text{ mmol L}^{-1} \text{min}^{-1} \text{g}^{-1}$) as a result of a better infiltration. As a conclusion, 3D-fiber samples are more efficient than flat glass substrates due to higher specific surface areas. However the microstructure of TiO₂ has also to be optimized. It is possible to increase the number of active sites, and thus the photocatalytic activity, only by changing the microstructure (crystal size, porosity) and thickness of the film.

The anionic doping of these infiltrated MOCVI TiO₂ films is in progress starting from the results presented in companion papers [38,39] in order to get photocatalytic activity in the visible range. Indeed the glass micro-fibers used as support are transparent to visible light and this might subdue the effects of shading observed under UV irradiation. The thickness (related to the amount) of photocatalyst could be then optimized to produce new media for specific applications.

5. Conclusions

The photocatalytic efficiency of MOCVD and MOCVI TiO₂ thin films was evaluated for different pollutants in aqueous solution (imazapyr, malic acid, orange G) and in air stream (toluene). In all cases the initial decomposition rate r_0 of the pollutants increases almost linearly with the film thickness and reaches a limit (critical thickness above which the film thickness has no influence). This limit is due to the depth penetration of the light and its value is strongly related to the micro-structural characteristics of the films. TiO₂ layers deposited at 400–500 °C show the best PA. They exhibit a high porosity (50–55%), a columnar morphology and a high specific surface area ($17 \text{ m}^2 \text{g}^{-1}$). A significant increase of the film porosity was achieved by changing the substrate geometry, i.e. substitution of flat glass plates by glass micro-fibers (highly curved surface). This leads to saturation of the PA at lower film thickness but the efficiency of the PA normalized to the mass of photocatalyst is increased by a factor five. The lower critical thickness results from UV light absorption and scattering effects in the porous samples. The same critical thickness was observed for films tested using pollutants dispersed in water (orange G) and air (toluene), giving evidence that film microstructure also governs the efficiency of the photocatalytic process. Moreover, high pollutant decomposition rates were achieved by well TiO₂-infiltrated samples of micro-fibrous media (orange G aqueous solution, toluene vapor). The large dispersion and the conformal coverage of the fiber fabric led to a high number of available photocatalytic sites. Complete photocatalyst regeneration was achieved after UV irradiation under oxygen stream for 24 h thereby increasing significantly the efficiency and life time of the photocatalyst.

Appendix A. Supplementary data

Supplementary data associated with this article can be found, in the online version, at [doi:10.1016/j.apcatb.2009.05.029](https://doi.org/10.1016/j.apcatb.2009.05.029).

References

- [1] S. Hager, R. Bauer, *Chemosphere* 38 (1999) 1549.
- [2] A. Vohra, D.Y. Goswami, D.A. Deshpande, S.S. Block, *Appl. Catal. B* 64 (2006) 57.
- [3] I.K. Konstantinou, T.A. Albanis, *Appl. Catal. B* 42 (2003) 319.
- [4] J.-M. Herrmann, *Catal. Today* 53 (1999) 115.
- [5] K.-M. Schindler, M. Kunst, *J. Phys. Chem.* 94 (1990) 8222.
- [6] M. Maeda, T. Watanabe, *Surf. Coat. Technol.* 201 (2007) 9309.
- [7] Y. Ku, R.-M. Leu, K.-C. Lee, *Wat. Res.* 30 (1996) 2569.
- [8] F.-D. Duminica, F. Maury, F. Senocq, *Surf. Coat. Technol.* 188–189 (2004) 255.
- [9] F.D. Duminica, F. Maury, R. Hausbrand, *Surf. Coat. Technol.* 201 (2007) 9304.
- [10] D. Robert, A. Piscopo, O. Heintz, J.V. Weber, *Catal. Today* 54 (1999) 291.
- [11] B. Herbig, P. Lobmann, *J. Photochem. Photobiol. A* 163 (2004) 359.
- [12] S.-C. Jung, B.-H. Kim, S.-J. Kim, N. Imaishi, Y.-I. Cho, *Chem. Vap. Deposition* 11 (2005) 137.
- [13] C.-S. Kim, I.-M. Kwon, B.K. Moon, J.H. Jeong, B.-C. Choi, J.H. Kim, H. Choi, S.S. Yi, D.-H. Yoo, K.-S. Hong, J.-H. Park, H.S. Lee, *Mater. Sci. Eng. C* 27 (2007) 1343.
- [14] C. Sarantopoulos, A.N. Gleizes, F. Maury, *Surf. Coat. Technol.* 201 (2007) 9354.
- [15] C. Sarantopoulos, F. D. Duminica, A. N. Gleizes, F. Maury, *Electrochem. Soc. Proc. Volume, (EUROCVI 15)*, A. Devi, R. Fischer, H. Parala, M. Allendorf, M. Hitchman (Eds.), *The Electrochem. Soc.*, Pennington, NJ, 09 (2005) 252.
- [16] J.C. Manificier, J. Gasot, J.P. Fillard, *J. Phys. E: Sci. Instrum.* 9 (1976) 1002.
- [17] O.S. Heavens, *Optical Properties of Thin Solid Films*, second ed., Dover Publications Inc., 1991.
- [18] M. Sreemany, S. Sen, *Mater. Chem. Phys.* 83 (2004) 169.
- [19] M. Born, E. Wolf, *Principle of Optics*, Pergamon, New York, 1975.
- [20] C. Guillard, D. Debayle, A. Gagnaire, H. Jaffrezic, J.-M. Herrmann, *Mater. Res. Bull.* 39 (2004) 1445.
- [21] M. Carrier, N. Perol, J.-M. Herrmann, C. Bordes, S. Horikoshi, J.O. Paise, R. Baudot, C. Guillard, *Appl. Catal. B* 65 (2006) 11.
- [22] K.L. Siefering, G.L. Griffin, *J. Electrochem. Soc.* 137 (1990) 814.
- [23] R. Jenkins, R.L. Snyder, *Introduction to X-ray Powder Diffractometry*, John Wiley & Sons, New York, 1996.
- [24] R. Marchand, L. Brohan, M. Tournoux, *Mater. Res. Bull.* 15 (1980) 1129.
- [25] D.-L. Shieh, C.-H. Ho, J.-L. Lin, *Microporous Mesoporous Mater.* 109 (2008) 362.
- [26] M.L. Hitchman, F. Tian, *J. Electroanal. Chem.* 538–539 (2002) 165.
- [27] A.J. Maira, K.L. Yeung, C.Y. Lee, P.L. Yue, C.K. Chan, *J. Catal.* 192 (2000) 185.
- [28] M. Fallet, S. Permpoon, J.L. Deschanvres, M. Langlet, *J. Mater. Sci.* 41 (2006) 2915.
- [29] C.J. Taylor, D.C. Gilmer, D.G. Colombo, G.D. Wilk, S.A. Campbell, J. Roberts, W.L. Gladfelter, *J. Am. Chem. Soc.* 121 (1999) 5220.
- [30] S.A. Larson, J.L. Falconer, *Catal. Lett.* 44 (1997) 57.
- [31] R. Mendez-Roman, N. Cardona-Martinez, *Catal. Today* 40 (1998) 353.
- [32] S.B. Kim, S.C. Hong, *Appl. Catal. B* 35 (2002) 305.
- [33] Y. Luo, D.F. Ollis, *J. Catal.* 163 (1996) 1.
- [34] T. Ibusuki, K. Takeuchi, *Atmos. Environ.* 20 (1986) 1711.
- [35] C. Young, T.M. Lim, K. Chiang, *R. Amal, Water Sci. Technol.* 50 (2004) 251.
- [36] M.C. Blount, J.L. Falconer, *Appl. Catal. B* 39 (2002) 39.
- [37] T.N. Obee, R.T. Brown, *Environ. Sci. Technol.* 29 (1995) 1223.
- [38] F.-D. Duminica, F. Maury, R. Hausbrand, *Surf. Coat. Technol.* 201 (2007) 9349.
- [39] C. Sarantopoulos, A. N. Gleizes, F. Maury, *Thin Solid Films*, [doi:10.1016/j.tsf.2009.04.070](https://doi.org/10.1016/j.tsf.2009.04.070).